

Low-energy electron–argon scattering in a low-frequency laser field

C-T Chen and F Robicieux

Department of Physics, Auburn University, Auburn, AL 36849, USA

Received 14 September 1995

Abstract. We have used several non-perturbative Floquet methods to calculate the differential and total cross sections for electron scattering from argon in a CO₂ laser field. One method utilizes the mixed-gauge *R*-matrix technique to calculate the scattering cross section. A diabatic approximation adopted from molecular applications is also applied to this low-frequency limit. Results are compared with the well known Kroll–Watson approximation. We find that all three theoretical treatments agree well with each other but do not agree with some experimental results. Possible explanations for the discrepancy between the calculations and experiments are examined.

1. Introduction

The development of the laser not only provides a tool to examine atomic systems, it can also generate new phenomena by adding laser beams to some well studied processes. When a laser is combined with a collision process, new processes can occur, e.g. simultaneous electron–photon excitation (Mason 1993) or the strong modification field-free processes. The latter are known as laser-assisted processes. The experimental results to be examined in this paper belong to the laser-assisted category.

The development of theoretical techniques to study laser-assisted processes has not kept pace with the experiments partly because experimental laser intensities have increased significantly and invalidated perturbative approaches. A classic theoretical treatment of laser-assisted electron scattering from an atom was provided by Kroll and Watson (1973). Since then it has been an important tool as a guide for the analysis of experimental data. The Kroll–Watson approximation (KWA) is a non-perturbative method for calculating laser-assisted scattering cross sections and is widely used in analysing experimental data. One of the advantages of the Kroll–Watson formalism is the extraordinary simplicity of the formulae for the cross sections. According to the KWA, the free–free transitions are most likely to occur if the momentum transfer \mathbf{Q} of the electron is aligned with the polarization direction $\hat{\mathbf{e}}$ of the laser field. The experimental set-up for this situation can be achieved in two ways. One is to inject the electron in the direction $\hat{\mathbf{e}}$ and measure free–free signals at large scattering angles. The other arrangement is to rotate both the electron gun and the detector to make the momentum transfer \mathbf{Q} align with $\hat{\mathbf{e}}$. In both cases, $\hat{\mathbf{e}} \cdot \mathbf{Q}$ is substantially different from zero. The KWA has been reported to have fair agreement with the experiments for these cases.

Recent experiments performed by Wallbank and Holmes (1993, 1994) have specifically explored the situation where $\hat{\mathbf{e}} \cdot \mathbf{Q} \approx 0$. The arrangements of the experiment are therefore different from that described above. In the first case, the detector is placed at small angles.

In the second case, the laser beam enters the scattering region in a direction such that its polarization direction $\hat{\epsilon}$ bisects the angle between the incident direction and outgoing direction of the electron. The low-frequency KWA formula has a simple form. The cross section for absorbing n photons is mainly described by a product of the field-free elastic cross section and the square of the regular Bessel function $J_n(\lambda)$. The argument of the Bessel function, λ , is proportional to $\hat{\epsilon} \cdot \mathbf{Q}$ and the order n corresponds to n -photon processes. For small arguments, $J_n(\lambda) \approx \lambda^n / 2^n n!$ and under experimental conditions with $\hat{\epsilon} \cdot \mathbf{Q} \approx 0$, the KWA is either not valid or it predicts tiny free-free cross sections (this is discussed in section 2.3). Therefore, it is very interesting that the experiments showed relatively strong signals in both arrangements where $\hat{\epsilon} \cdot \mathbf{Q} \approx 0$. The measured cross section is several orders of magnitude greater than the prediction of the KWA. These experiments seem to demonstrate that the KWA is not adequate in describing the free-free transition for *some* experimental conditions. The main purpose of this paper is to present several calculations for the case $\hat{\epsilon} \cdot \mathbf{Q} \approx 0$ in order to judge the reliability of the theoretical methods and the assumptions on which they are based.

Unfortunately, we have not found a mechanism to explain the discrepancy between calculated and experimental free-free cross sections when $\hat{\epsilon} \cdot \mathbf{Q}$ is small. All of our calculated cross sections are much smaller than experimental results. Several speculations about possible mechanisms invalidating the KWA have been discussed. The most promising speculation concerns the interaction of the incident electron with the polarization potential of the atom induced by the laser field. The KWA does not consider the *modification* of the interaction between the target atom and incident electron caused by the laser field; the atomic dipole moment induced by the laser field has been ignored in the KWA. Recently Rabadán *et al* (1994) examined the electron scattering from He at a 9° angle using a semiclassical method with a model potential. They confirmed the validity of the KWA under the experimental conditions. They also examined the laser-induced target polarization and concluded that it is negligible. However, there has been some evidence that this potential can dramatically influence the free-free cross section in the forward scattering direction (Byron *et al* 1984, 1987, Fainstein and Maquet 1994). In experimental studies of the resonance structures in free-free transitions of electron-neon and electron-argon scattering, Bader (1986) found a strong non-resonant background in the scattering at small angles. Such a background is especially pronounced in experiments with argon (but weak in neon) and cannot be described by the KWA. Argon has a relatively large polarizability compared to neon. The laser-induced dipole potential is proportional to the polarizability and therefore seems to fit the speculation that atomic polarizability can strongly enhance the cross section. In order to examine the problem closely, we have performed a non-perturbative calculation that incorporates the R -matrix method with Floquet expansion and scattering formulation to obtain the free-free differential cross section. We also introduce a diabatic approximation adopted from molecular applications and apply it to this low-frequency problem. Both approaches are compared to the experiments and also to the classic Kroll-Watson approximation.

2. Calculation methods

2.1. Floquet R -matrix

Recently, we proposed a mixed-gauge approach (Robicheaux *et al* 1995) to tackle the problem of electrons interacting with atoms/ions and laser fields. We briefly outline its main ingredients in this section. The usual approach to the interaction of an atomic

system with a laser field is to write the Schrödinger equation in one of the pure gauges (length, velocity, ‘acceleration’). These three pure gauges are suitable for the electron–laser interaction at short distances, intermediate distances and large distances, respectively (Dörr *et al* 1992, 1993, 1995). The Schrödinger equation is relatively simple in each of the three gauges. Although the Hamiltonian is simple in the ordinary gauges, the effect of the laser on the wavefunction has unfortunate properties that impede the implementation of the usual scattering techniques. Only in the acceleration gauge do the channels decouple at large distances and the scattering wavefunctions can be obtained. However, this gauge has difficulties if the potential has a singularity near $r = 0$. The acceleration gauge is only adequate for the problems in which the electron wavefunctions do not extend to small distances. For more general cases where the wavefunctions extend to all space, a natural approach is to obtain the wavefunctions in a length gauge near the nucleus, velocity gauge at intermediate distances and acceleration gauge at large distances. By matching the wavefunctions at the boundaries of the different gauge transformations, the wavefunctions for all space can be obtained.

The mixed-gauge method maintains the spirit of the pure-gauge approach by adopting suitable gauges in different regions. However, the gauges are introduced smoothly over a range of distances. In this way, part of the electron–laser interaction is incorporated analytically into the wavefunctions. By introducing the gauges in a smooth manner it may help to eliminate possible cusplike problems in the wavefunctions.

The wavefunction of an electron in a laser field is a solution of the equation

$$\left[\frac{1}{2}(\mathbf{p} + \mathbf{A}(t)/c)^2 + V(\mathbf{r})\right]\Psi(\mathbf{r}, t) = H\Psi(\mathbf{r}, t) = i\frac{\partial}{\partial t}\Psi(\mathbf{r}, t) \quad (1)$$

where $V(\mathbf{r})$ is the static potential and $\mathbf{A}(t) = \mathbf{A}_0 \sin(\omega t)$ is the vector potential of the laser field with frequency ω . We choose to solve for the wavefunctions with the form

$$\Psi_{Ej}(\mathbf{r}, t) = \exp\left(-iEt - i\int^t dt' \mathbf{A}(t') \cdot \mathbf{A}(t')/2c^2\right) e^{-i\phi(\mathbf{r}, \mathbf{p}, t)} \psi_{Ej}(\mathbf{r}, t) \quad (2)$$

where the unitary phase operator of the gauge transformation is chosen as

$$\phi(\mathbf{r}, \mathbf{p}, t) = -[G(\mathbf{r})\mathbf{A}_0 \cdot \mathbf{p} + \mathbf{A}_0 \cdot \mathbf{p}G(\mathbf{r})]\cos(\omega t)/2c\omega. \quad (3)$$

The parameter E denotes the electron’s energy when it has not absorbed or emitted any photons. The factor $G(\mathbf{r}) = \{1 - \exp(-\beta(r - r_c)^4)\}\Theta(r - r_c)$ prevents gauge transformation at small distances but allows the transformation from the velocity gauge to the acceleration gauge at large distances. $\Theta(r - r_c)$ indicates we begin this transformation at a distance r_c which we choose to be several times larger than $A_0/c\omega$, the amplitude of the oscillation of the potential in the acceleration gauge. β should be as small as possible but needs to be large enough to ensure the Schrödinger equation is completely in the acceleration gauge at the R -matrix boundary (i.e. $G(r_0) \approx 1$ within tolerable error where r_0 is the size of the R -matrix). In equation (3) we have omitted the possibility for making the length gauge to velocity gauge transformation at small distances in order to simplify evaluations of the matrix elements involving commutators of the phase operator with the Hamiltonian. The phase operator satisfies the commutation relation $[\phi, \partial\phi/\partial t] = 0$ and the $\psi_{Ej}(\mathbf{r}, t)$ satisfies the simplified equation

$$E\psi_{Ej}(\mathbf{r}, t) = (\bar{H} - \mathbf{A}(t) \cdot \mathbf{A}(t)/2c^2)\psi_{Ej}(\mathbf{r}, t) \quad (4)$$

where

$$\bar{H} = H - \frac{\partial \phi}{\partial t} - i \frac{\partial}{\partial t} + [i\phi, H] + \frac{1}{2!} [i\phi, [i\phi, H]] + \dots \quad (5)$$

The wavefunction $\psi_{Ej}(\mathbf{r}, t)$ is constructed using a Floquet expansion

$$\psi_{Ej}(\mathbf{r}, t) = \sum_{j'} \exp(-i\omega n_{j'} t) Y_{l_{j'} m_{j'}}(\theta, \varphi) \psi_{Ej', j}(r) \quad (6)$$

in which $\psi_{Ej', j}(r)$ has the asymptotic form

$$\psi_{Ej', j}(r) = f_{j'}(r) \delta_{j', j} + \sqrt{2} f_{j'}^+(r) T_{j', j} \quad r \geq r_0. \quad (7)$$

We have used the symbol $f_{j'}^+ = (-g_{j'} + i f_{j'})/\sqrt{2}$ where f and g are the regular and irregular solutions of the radial Schrödinger equation with zero potential. For short-ranged potentials such as electron scattering from neutral atoms (the present case), f and g represent the energy normalized regular and irregular spherical Bessel functions, respectively. The construction of the radial functions, $\psi_{Ej', j}(r)$, can be accomplished using many methods. We use the variational R -matrix method (Schneider 1975, Greene 1985, Robicheaux 1991) in which we expand the Hamiltonian in a set of basis functions which do not all have the same logarithmic derivative on the boundary. In the variational principle, the $\mathbf{p}^2 + \text{Bloch}$ operator in the Hamiltonian is replaced by $\mathbf{p}^\dagger \mathbf{p}$.

The advantage of the proposed mixed-gauge approach is that it converges quickly with respect to the number of Floquet blocks. Also, it allows us to obtain the scattering parameters with the usual R -matrix method. We have found that this method gives accurate results as long as $A_0/c\omega$ is small compared to the size of the R -matrix boundary. The disadvantage of the mixed gauge is that at any distance the Schrödinger equation is not in one of the pure gauges and consequently the Hamiltonian is more complicated than it is in a pure gauge. When $A_0/c\omega$ becomes large, the expansions of the higher-order commutators in the Hamiltonian pose difficulties. In our calculations, we have evaluated $[i\phi, H]$ analytically and the next order $[i\phi, [i\phi, H]]$ numerically by matrix multiplication. We have found (by keeping the second-order commutator of the phase operator with the Hamiltonian) that the Floquet calculation is reliable if the amplitude $A_0/c\omega$ is less than 10% of the R -matrix size r_0 .

2.2. Diabatic approximation

In the acceleration gauge the potential oscillates along the direction of the polarization with a time-dependent amplitude given by $\alpha(t) = \hat{z}(A_0/c\omega) \cos \omega t$ in au. Since the frequency of the laser is small, the incident electron may be moving much faster than the oscillation of the potential. If the time it takes the electron to scatter from the potential is small compared to the laser period, we may treat the potential as fixed at the time when the scattering occurs. This approximation to the wavefunction will only be good up to distances less than v/ω where v is the electron's speed. For the experiments discussed below, $v/\omega \sim 178$ au. The scattered waves are spherical waves centred at the origin of the potential at that time and can be written as

$$\psi_{Elm}(\mathbf{R}, t) = e^{-iEt} Y_{lm}(\hat{R}) [j_l(kR) - y_l(kR) \tan \delta_l] \quad (8)$$

where \mathbf{R} is the position vector from the potential to the electron. We may obtain the spherical wavefunctions centred at the true origin by using the re-expansion formula (Danos and Maximon 1965, Dill and Dehmer 1974) which is expressed as

$$\begin{aligned} \begin{pmatrix} j_l(kR) \\ y_l(kR) \end{pmatrix} Y_{lm}(\hat{\mathbf{R}}) &= \sum_{LM\lambda\mu} i^{L+\lambda-l+2m} \sqrt{4\pi} \sqrt{(2L+1)(2l+1)(2\lambda+1)} \\ &\times \begin{pmatrix} L & l & \lambda \\ 0 & 0 & 0 \end{pmatrix} \begin{pmatrix} L & l & \lambda \\ M & -m & \mu \end{pmatrix} j_\lambda(k|\boldsymbol{\alpha}(t)|) Y_{\lambda\mu}(\hat{\boldsymbol{\alpha}}(t)) \begin{pmatrix} j_L(kr) \\ y_L(kr) \end{pmatrix} Y_{LM}(\hat{\mathbf{r}}). \end{aligned} \quad (9)$$

In the equation, \mathbf{r} is the relative position of the electron to the true origin and $\boldsymbol{\alpha}(t)$ points from the potential to the true origin. The relationship among three position vectors is $\mathbf{R} = \mathbf{r} + \boldsymbol{\alpha}(t)$. In this formula, the amplitude $\boldsymbol{\alpha}(t)$ is assumed to be smaller than the distance r from the electron to the centre of the potential. The wavefunction now depends explicitly on \mathbf{r} and is written in a compact form

$$\psi_{Elm}(\mathbf{r}, t) = e^{-iEt} \sum_{LM} Y_{LM}(\hat{\mathbf{r}}) [j_L(kr) I_{LM,lm}(t) - y_L(kr) J_{LM,lm}(t)] \quad (10)$$

where we have used $j(kr)$ and $y(kr)$ to denote explicitly the spherical Bessel functions for the present short-ranged interaction between electron and argon. The matrix $I_{LM,lm}(t)$ is obtained from (9) as

$$\begin{aligned} I_{LM,lm}(t) &= \sum_{\lambda\mu} i^{L+\lambda-l+2m} \sqrt{4\pi} \sqrt{(2L+1)(2l+1)(2\lambda+1)} \\ &\times \begin{pmatrix} L & l & \lambda \\ 0 & 0 & 0 \end{pmatrix} \begin{pmatrix} L & l & \lambda \\ M & -m & \mu \end{pmatrix} j_\lambda(k|\boldsymbol{\alpha}(t)|) Y_{\lambda\mu}(\hat{\boldsymbol{\alpha}}(t)) \end{aligned} \quad (11)$$

and $J_{LM,lm}(t)$ is related to $I_{LM,lm}(t)$ simply by

$$J_{LM,lm}(t) = I_{LM,lm}(t) \tan \delta_l(E). \quad (12)$$

The parameter $\delta_l(E)$ represents the phase shift of the electron due to the presence of the atom at position $\boldsymbol{\alpha}(t)$. It is obtained by the usual potential scattering method with a model potential to be described later. The $I_{LM,lm}(t)$ is a continuous function of t ; although $j_\lambda(k|\boldsymbol{\alpha}(t)|)$ and $Y_{\lambda\mu}(\hat{\boldsymbol{\alpha}}(t))$ are separately discontinuous, their product is continuous. Since the oscillation of the potential is along the direction of the polarization of the laser field which is chosen as \hat{z} , the μ in the above expressions is simply zero. As a result, different M and m do not mix in the transformation. We can use a single index m and move it from a subscript to a superscript and denote the matrices as $I_{L,l}^m(t)$ and $J_{L,l}^m(t)$, respectively, for a particular m . These two matrices suffice to construct the transition matrix $T_{L,L'}^m(t)$ at the time when the scattering occurs. Alternatively, because $J_{L,l}^m(t)$ is related to $I_{L,l}^m(t)$, we can obtain $T_{L,L'}^m(t)$ from

$$T_{L,L'}^m(t) = \sum_l I_{L,l}^m(t) I_{L',l}^m(t) \sin \delta_l e^{i\delta_l}. \quad (13)$$

Using the T -matrix and imposing the time-dependent part in the n' channel, we have the scattering wave

$$\psi_{En'lm}(\mathbf{r}, t) = e^{-iEt} e^{-in'\omega t} \sum_L Y_{Lm}(\hat{\mathbf{r}}) [j_L(kr) \delta_{Ll} + h_L^+(kr) T_{L,l}^m(t)] \quad (14)$$

where $h_L^+(kr) = j_L(kr) + iy_L(kr)$ is the spherical Hankel function of the first kind. At large distances, the asymptotic form of the Floquet wavefunction in channel n' is

$$\psi_{En'lm}(\mathbf{r}, t) = e^{-iEt} \sum_{nL} Y_{Lm}(\hat{\mathbf{r}}) e^{-in\omega t} [j_L(k_n r) \delta_{Ll} \delta_{nn'} + h_L^+(k_n r) T_{nL, n'l}^m]. \quad (15)$$

This form holds for distances larger than the size of the atom plus $A_0/c\omega$. Furthermore, because $\omega \ll 1$ and $k_n = \sqrt{2(E + n\omega)} \approx k + n\omega/k$ where $k = \sqrt{2E}$, $j_L(k_n r) \approx j_L(kr) + dj_L(kr)/d(kr) \cdot r/(k/n\omega)$. The derivative, $j_L'(z)$, is roughly the same size as $j_L(z)$ and as long as $r < (k/n\omega)$, we may approximate $j_L(k_n r) \approx j_L(kr)$ and $h_L^+(k_n r) \approx h_L^+(kr)$ for any n . The approximation of the wavefunction is valid for distances less than $v/n\omega$ as described above (8). Applying the frame transformation to (14) to match Floquet wavefunction (15), we get two relations

$$j_L(k_n r) \delta_{nn'} = j_L(kr) \frac{\omega}{2\pi} \int_0^{2\pi/\omega} e^{i(n-n')\omega t} dt \quad (16)$$

and

$$T_{nL, n'L'}^m = \frac{\omega}{2\pi} \int_0^{2\pi/\omega} T_{L, L'}^m(t) e^{i(n-n')\omega t} dt. \quad (17)$$

Equation (16) is an identity under the assumption we have made. Equation (17) gives the time-independent Floquet T -matrix $T_{nL, n'L'}^m$ and can be used to obtain cross sections. From equation (17), it is clear that the T -matrix elements are the same for channels with $(n - n')$ and $-(n - n')$. Usually we are interested in the incident channel $n' = 0$ and the exit channel n . The T -matrix elements are therefore symmetric for the emission process ($n < 0$) and the absorption process ($n > 0$). Consequently, we have exactly the same cross section for emission and absorption in the diabatic approximation. This is one of the special properties of this approximation and is a consequence of the low-frequency assumption. This symmetry is not exactly obeyed for the exact wavefunction but can be considered a good rule of thumb.

2.3. Kroll–Watson approximation

In their original paper, Kroll and Watson derived a free–free differential cross section valid for low frequencies. In this limit, the differential cross sections for an electron scattering from a potential and absorbing n photons is given by

$$\frac{d\sigma_n}{d\Omega} = \frac{k_f}{k_i} J_n^2(\lambda) \frac{d\sigma_{\text{el}}(\varepsilon, \mathbf{Q})}{d\Omega} \quad (18)$$

where k_i and k_f are the magnitudes of the initial and final momentum, respectively. For emission of n photons, replace n with $-n$. J_n is the ordinary Bessel function of order n , $\lambda = A_0 \hat{\mathbf{e}} \cdot \mathbf{Q}/c\omega$ and $d\sigma_{\text{el}}/d\Omega$ is the differential cross section of elastic scattering in the absence of laser fields. The elastic scattering cross section is to be evaluated at an energy

$$\varepsilon = E_i - n\omega(\hat{\mathbf{e}} \cdot \mathbf{k}_i/\hat{\mathbf{e}} \cdot \mathbf{Q}) + (n\omega)^2/2(\hat{\mathbf{e}} \cdot \mathbf{Q})^2 \quad (19)$$

with E_i the incident energy and $\mathbf{Q} = \mathbf{k}_f - \mathbf{k}_i$, the momentum transfer. The expression for the energy ε is valid for $|n/\lambda| \leq 1$. For the conditions where $\hat{\mathbf{e}} \cdot \mathbf{Q} \approx 0$ this approximation fails. Often in the application of analysing experimental data the energy is replaced by

$$\varepsilon = E_i + n\omega \quad (20)$$

at which the elastic cross section is calculated. This replacement always gives $d\sigma_{\text{el}}(\varepsilon, \mathbf{Q})/d\Omega \approx d\sigma_{\text{el}}(E_i, \mathbf{Q})/d\Omega$ in the low-frequency limit and the ratio of the free–free transition to the elastic scattering is determined by $J_n^2(\lambda)$. For $\hat{\mathbf{e}} \cdot \mathbf{Q} \approx 0$, the free–free cross section is always a tiny fraction of the field-free cross section which is reflected in the KWA.

3. Model potential

The majority of our calculations are for the low-energy region where the incident electron energy is well below the excitation energy of Ar atoms. Without the presence of the laser field the process is simply elastic scattering. With an intensity of $0.38 \times 10^8 \text{ W cm}^{-2}$ and a low frequency 0.0043 au, the atomic potential of Ar is modified only slightly by the laser field. To a good approximation, we may assume the potential is described by the elastic electron scattering. Many experiments and theoretical analyses have provided accurate phase shifts for low incident energies (Williams 1979, Fon *et al* 1983, McEachran and Stauffer 1983, Furst *et al* 1989). Since the atomic structure does not play a dynamic role, we replace the effect of the 18 Ar electrons on the incident electron with a local, model potential. In section 5, we will examine the effects of this approximation. The potential in our calculation is assumed to have the analytical form

$$V(r) = -\frac{Z}{r} e^{-\alpha_1 r} - \alpha_2 e^{-\alpha_3 r} - \frac{\alpha_d}{2r^4} [1 - e^{-(r/r_{\text{cut}})^3}]^2 \quad (21)$$

where Z is the nuclear charge, α_d is the static electric polarizability and r_{cut} is the cut-off distance for the polarized potential induced by the incident electron. α_i are parameters, together with r_{cut} , to be determined by minimizing the differences between the elastic differential cross sections from potential $V(r)$ and from the phase-shift analysis of the experiment (Furst *et al* 1989). For Ar, $Z = 18$, $\alpha_d = 10.77$ (Johnson *et al* 1983) and the minimization gives $\alpha_1 = 3.04$, $\alpha_2 = 10.62$, $\alpha_3 = 1.83$ and $r_{\text{cut}} = 1.76$ au.

An atom exposed to a low-frequency monochromatic laser with linear polarization is polarized and classically gives rise to an electric dipole potential

$$V_{\text{pol}}(r) = \alpha_d E_0 \cos \theta \cos \omega t / r^2. \quad (22)$$

The field strength E_0 is related to A_0 by $E_0 = A_0 \omega / c$ and $E_0 = 3.3 \times 10^{-5}$ au for the experimental intensity and frequency. This potential is included in the R -matrix calculation and we will investigate its long-range effect in a later section.

4. Results

In the present calculation, we used Floquet blocks from $n = -6$ to 6 and angular-momentum states from $l = 0$ to 11 for each n . We used 20 radial basis functions for each n and l to represent the $\psi_{Ej,j}(r)$ inside the R -matrix boundary. The convergence was checked by calculating cross sections with a smaller range of n, l . We chose the size of the R -matrix to be 30 au for all of the calculations. A CO₂ laser has frequency 0.0043 au ($\hbar\omega = 0.117$ eV) and the intensity was set to $0.38 \times 10^8 \text{ W cm}^{-2}$ to match the experiments. The amplitude of the oscillating potential $A_0/c\omega$ is 1.78 au. The incident electron energy is 8 eV except where otherwise specified. The laser is assumed to be monochromatic, spatially homogeneous and linearly polarized.

4.1. Differential cross sections

Our results are presented in accordance with three different experimental arrangements by Wallbank and Holmes. (i) The incident electron direction k_i is parallel to the laser field polarization \hat{e} . (ii) The momentum transfer of the electron Q is always parallel to \hat{e} . (iii) The momentum transfer of the electron Q is always perpendicular to \hat{e} . In cases (ii) and (iii), both electron gun and detector need to be rotated for different scattering angles. For consistency, in all of the calculations we use the simplified formula (20) instead of (19) for the KWA. For cases (i) and (ii), much better agreement between the diabatic approximation and the KWA in the backward direction is obtained when (19) is used.

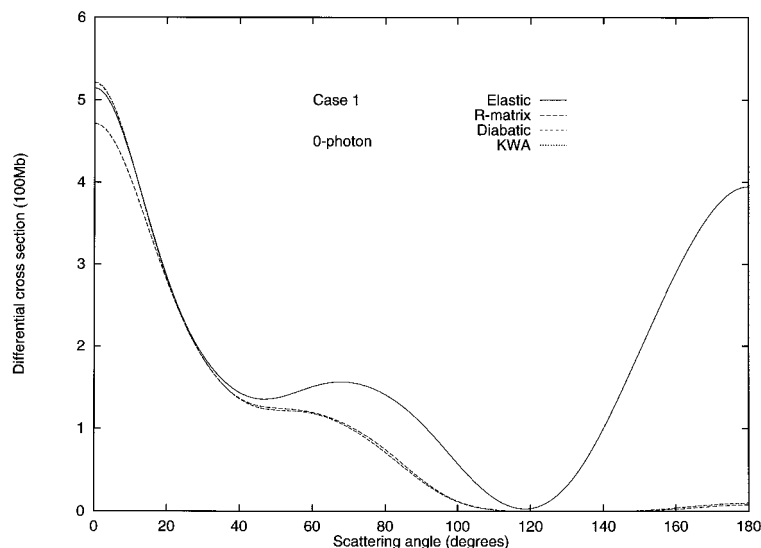


Figure 1. Zero-photon free-free differential cross section with the incident direction parallel to the polarization of the laser. The KWA curve overlaps with the diabatic curve and they are not distinguishable in this figure.

4.1.1. Case 1. $k_i \parallel \hat{e}$. Figure 1 shows the differential cross sections for all three different calculations for zero-photon free-free transition. The field-free elastic scattering cross section is plotted for comparison. The zero-photon process deviates from the elastic scattering only slightly at small scattering angles but significantly at large scattering angles. The zero-photon cross section is suppressed below the field-free cross section in the backward direction. The momentum transfer Q plays an important role in the free-free transition. Q is large at large scattering angles where free-free processes are likely to occur. One- and two-photon absorptions are shown in figures 2 and 3, respectively. The cross sections for emission processes (not shown) for the R -matrix calculation and the KWA are nearly equal to the cross sections for the absorption processes. This shows the validity of the diabatic approximation for which the absorption and emission cross sections are exactly equal. In the backward direction, the one- and two-photon cross sections are relatively large. This compensates for the reduction of the zero-photon process from elastic scattering in figure 1 at large scattering angles. Also it is interesting that the two-photon absorption is stronger than the one-photon absorption in the backward direction. This shows the non-perturbative nature of this scattering process. All cross sections show a minimum around 120° because the elastic scattering has a minimum at that angle.

The agreement of the R -matrix calculation with the other two methods for the one-photon process is not as good as that for the two-photon process, especially in the backward direction. This can be traced back to the truncation of the Hamiltonian in (5). We note the first commutator in the Hamiltonian is $[i\phi, H]$ and it can be expanded into three parts. They are $-(A_0/4c\omega) \cos \omega t [i(p_z G + G p_z), \mathbf{p}^2]$, $-(A_0/2c\omega) \cos \omega t [i(p_z G + G p_z), V]$ and $-(A_0^2/4c^2\omega) \sin 2\omega t [i(p_z G + G p_z), p_z]$. The first two cause one-photon transitions and the last causes two-photon transitions. As far as the interaction strength is concerned, only the first one is important. This can be easily seen since the function $G(r)$ turns the transformation into the acceleration gauge at large distances where the potential V is practically zero. The second term is therefore not important. The third term, apart

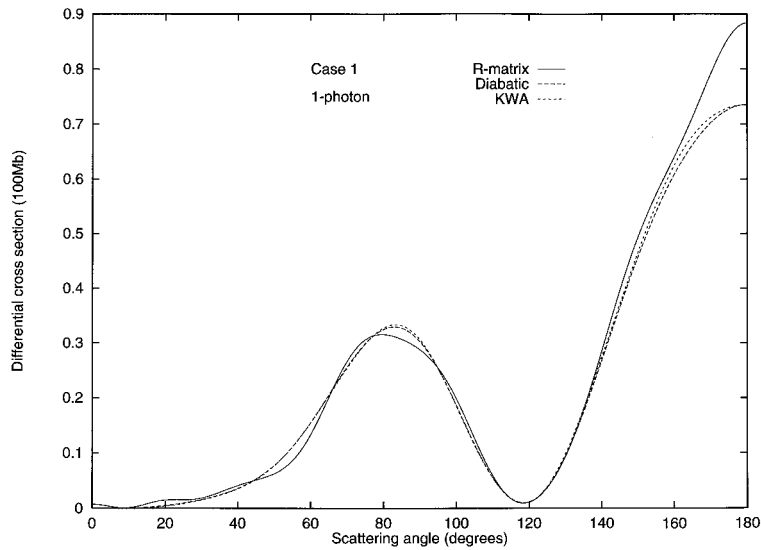


Figure 2. Same as figure 1 but for the one-photon absorption.

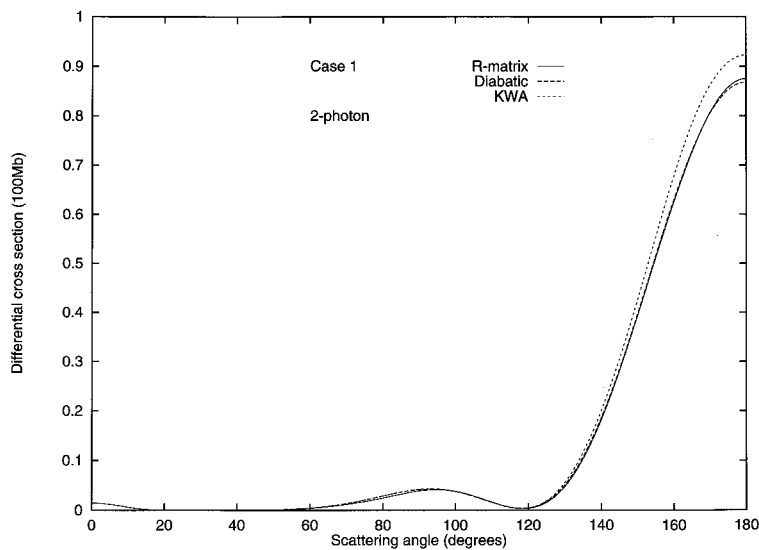


Figure 3. Same as figure 1 but for the two-photon absorption.

from the commutator, contains an additional factor A_0/c to the first term. For the frequency and intensity of the present case, this factor would reduce the contribution by two orders of magnitude. We also checked these three terms numerically and confirmed the dominance of the first. In short, the commutator $[i\phi, H]$ is a one-photon interaction in character for the experimental parameters. The phase operator $i\phi$ is also one-photon in origin since it is proportional to $\cos \omega t$. Therefore the next commutator $[i\phi, [i\phi, H]]/2$ basically contributes to zero-photon and two-photon transitions. We do not include the next commutator $[i\phi, [i\phi, [i\phi, H]]]/6$ and its followers in the R -matrix calculation. Therefore

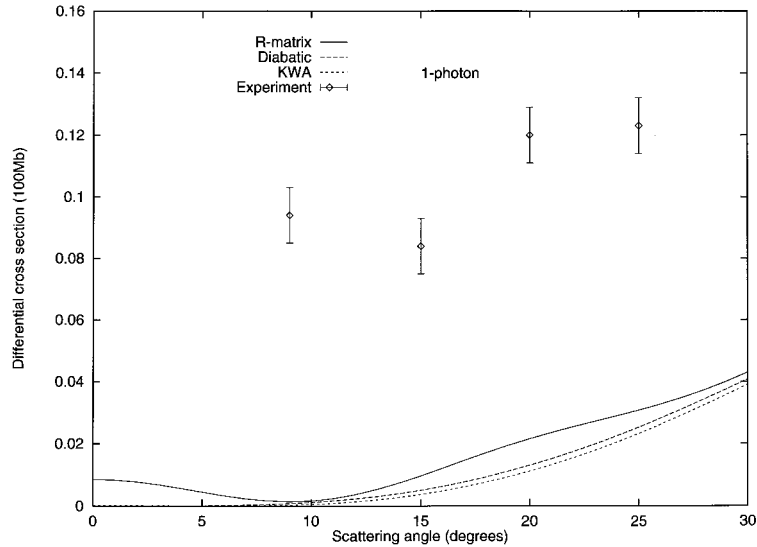


Figure 4. One-photon free-free differential cross section with the incident direction parallel to the polarization of the laser. The incident energy is 10.5 eV.

the leading term we have neglected is a one- and three-photon interaction. So the lowest-order interaction we have neglected in the Hamiltonian contributes to one-photon processes. This is why the two-photon cross section in the R -matrix calculation is better than that for the one-photon process.

For small scattering angles, all inelastic free-free transitions are predicted to have small cross sections. This can be seen from the KWA in which the argument of the Bessel function, λ , contains $\hat{\epsilon} \cdot \mathbf{Q}$ and the momentum transfer \mathbf{Q} is not only small itself but also nearly perpendicular to $\hat{\epsilon}$ at small angles. The R -matrix and diabatic approximation agree with the KWA but all fail to predict the experimental results at small scattering angles. This conclusion does not change if we increase the incident energy to 10.5 eV at which the experiment was performed in this geometric arrangement. In figure 4 we concentrate on small scattering angles and compare the calculations with the experiment. The experimental results are much larger than the calculations.

4.1.2. Case 2. $\mathbf{Q} \parallel \hat{\epsilon}$. One-photon and two-photon processes are shown in figures 5 and 6, respectively. The shape looks similar to that in case 1. But because the momentum transfer is arranged to favour the free-free transition, it begins to give appreciable signals at small angles. At large angles the quantity $\hat{\epsilon} \cdot \mathbf{Q}$ is even closer to that of case 1 and the similarity in cross sections between the two cases becomes apparent. Again all three calculations agree reasonably well.

At large scattering angles, the cross sections from KWA deviate from the R -matrix and diabatic calculations for the $n = 2$ channel in both this case and case 1. This is because we have used the renormalized energy $\varepsilon = E_i + n\omega$ to evaluate elastic scattering cross section. If the original expression (equation (19)) is used, the agreement of the three methods is excellent at large angles. However, in doing so, $\hat{\epsilon} \cdot \mathbf{Q}$ in the denominator of the energy expression will cause difficulties at small angles so we chose to avoid it.

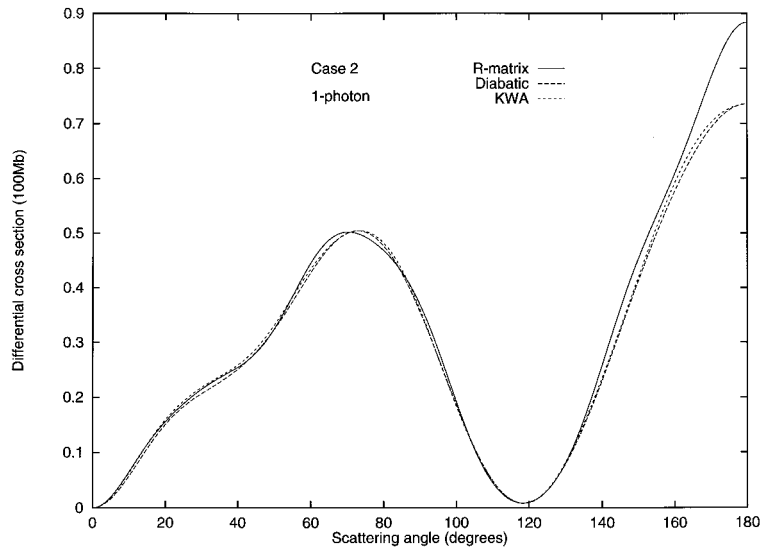


Figure 5. One-photon free–free differential cross section with the momentum transfer of the electron parallel to the polarization of the laser.

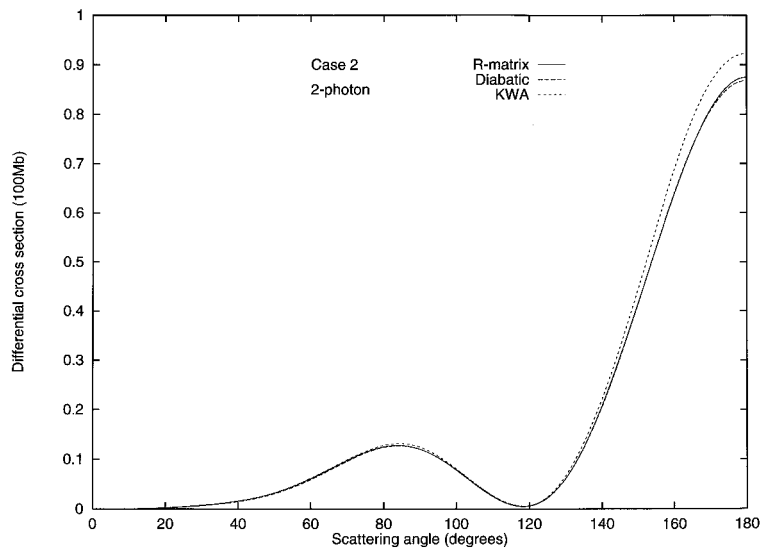


Figure 6. Same as figure 5 but for the two-photon absorption.

4.1.3. Case 3. $\mathbf{Q} \perp \hat{\epsilon}$. In this case the KWA fails to apply. The condition for the low-frequency limit is not satisfied. However, if the renormalized energy $\varepsilon = E_i + n\omega$ is used, the cross sections are calculable but tiny because of $\hat{\epsilon} \cdot \mathbf{Q} \approx 0$. The *R*-matrix method and the diabatic approximation are free from this limitation. The *R*-matrix calculation gives a very small cross section and the diabatic method has exactly zero cross section for one-photon absorption. The results are shown in figures 7 and 8. The two-photon process from the diabatic calculation has strong angular dependence but is too small to be displayed. The large

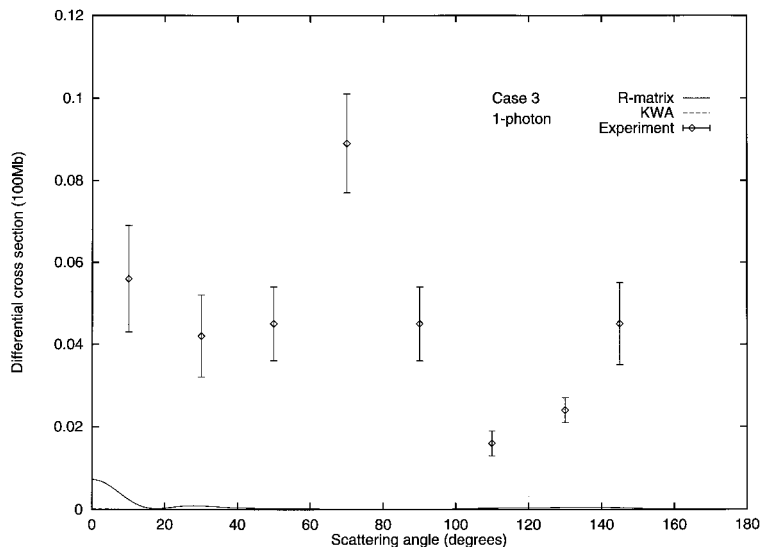


Figure 7. One-photon free-free differential cross section with the momentum transfer of the electron perpendicular to the polarization of the laser.

variation with angles actually comes from the incompleteness of angular-momentum states used in the calculation. By increasing l to 20, this ‘noise’ disappears. This may suggest that we need to include higher-angular-momentum states in the R -matrix calculation as well. However, the magnitude of this ‘noise’ in the R -matrix calculation is several orders of magnitude smaller than the cross section for non-perpendicular cases. Its magnitude is smaller than what has been truncated after the second commutator in the Hamiltonian. The one-photon transition from the diabatic calculation vanishes for a different reason to be discussed later. In the experiment both one- and two-photon cross sections have several per cent of the signals of the field-free scattering. It is at least two orders of magnitude larger than the R -matrix calculation. We leave the discussion of this discrepancy to a later section.

4.2. The sum rule

The sum rule for the free-free transition states is

$$\sum_n \frac{d\sigma_n}{d\Omega} = \frac{d\sigma_{el}}{d\Omega} \quad (23)$$

where the summation runs over all positive and negative n and the right-hand side is the field-free differential cross section. We find the R -matrix result follows this rule closely at large scattering angles but deviates slightly in the forward direction. The diabatic approximation, however, is consistent with the sum rule. The sum rule is known as a result of the low-frequency approximation (Mason 1993). In the limit $\omega \rightarrow 0$, the argument of the Bessel function is the same for emission and absorption process. By applying $\sum_n J_n^2(\lambda) = 1$, the sum rule follows. As we have mentioned, the diabatic approximation does not distinguish the absorption from emission process. This treatment is true only in the limit $\omega \rightarrow 0$. The diabatic approximation follows the sum rule more closely than the R -matrix calculation and

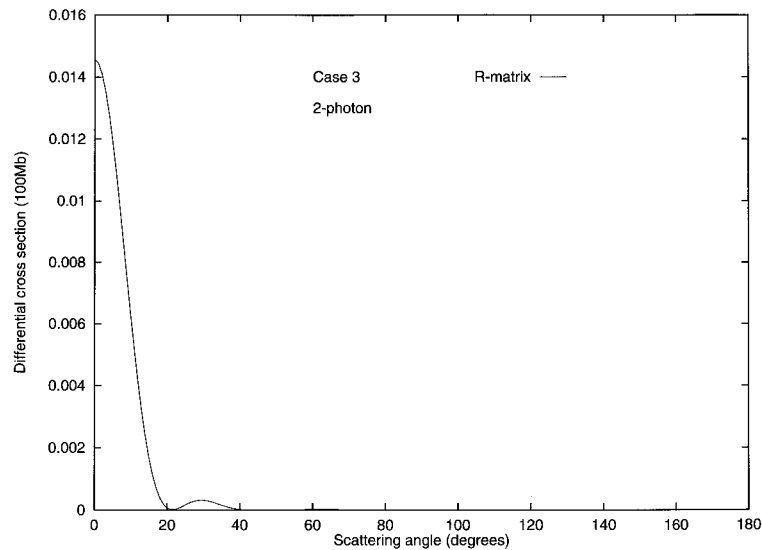


Figure 8. Same as figure 7 but for the two-photon absorption.

the KWA because it utilizes more low-frequency features in the approximation. The validity of the sum rule was reported to have other restrictions (Daniele *et al* 1986, 1987). The experimental parameters examined in this paper do not violate the restrictions.

4.3. Total cross sections

In this section we examine total cross sections for two experimental arrangements. The first one varies the incident angle of the electron gun with respect to the direction of laser polarization and collects all scattered electrons. The second one varies the angle between the detector and the laser polarization and shoots the incident electrons from all directions. The corresponding total cross sections are functions of the incident angle and the scattered angle, respectively. Although the polarization of the laser field defines a particular direction, there is no positive or negative distinction. The electron has the same probability to be scattered whether the incident angle is θ or $\pi - \theta$. Therefore we expect the total cross sections to be symmetric about 90° of the incident angle and of the scattered angle. The results shown in figure 9 confirm this general rule. The zero-photon total cross section has a maximum at 90° while the one-photon cross section has a minimum. The n -photon total cross section varies with angle but if we sum over all n -photon processes, including both absorption and emission, the angle dependence disappears. This result can be derived from the sum rule. The sum over all n -photon total cross sections is the integration over angular variables of (23). According to the sum rule, it is equal to the field-free total cross section which is independent of angle.

Is the angle dependence of the total cross sections the same for the two experimental arrangements? In the R -matrix calculation we found the angle dependence is approximately the same for the total cross section with respect to incident angle and scattered angle. They are exactly the same in the diabatic approximation. This may suggest that the symmetry of the angle dependence is a result of the low frequency of the laser. It may also be possible that the asymmetry between varying incident angle and scattered angle is caused by the truncation in the R -matrix calculation.

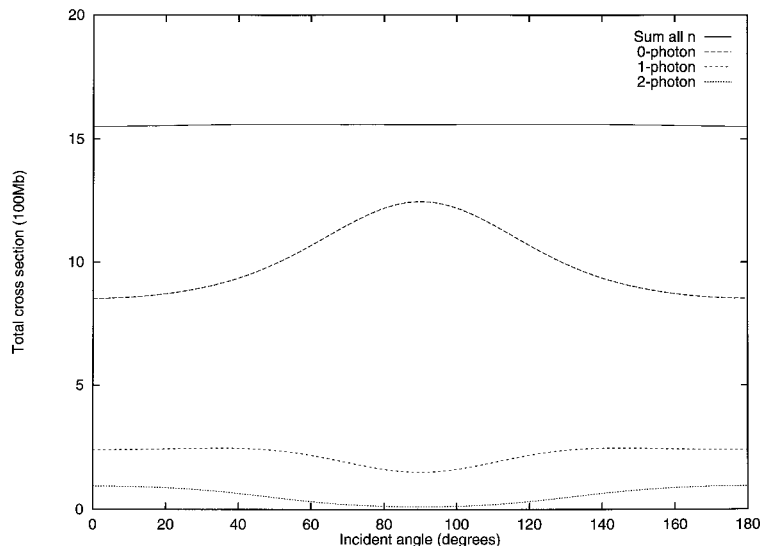


Figure 9. Total cross section as a function of the incident angle.

5. Discussion

We have found all three methods agree quite well under all experimental conditions. From the theoretical point of view this indicates that the low-frequency limit of the KWA and the diabatic approximation are valid since the R -matrix calculation is free from this limitation. But none of the methods predict the strong signals in the experiments when the product $\hat{\epsilon} \cdot \mathbf{Q}$ is small. It should be noted that the quantity $\hat{\epsilon} \cdot \mathbf{Q}$ appears explicitly in the KWA formula but implicitly through the p_z operator in the R -matrix formalism and through the transformation matrix $I_{L,l}^m(t)$ in the diabatic approximation.

If the experimental cross sections are correct, there must be some interactions that are missing in all three methods. Particularly, these interactions are pertinent to the observed cross section in the perpendicular case. Possible interactions responsible for the discrepancy, as suggested elsewhere, are the exchange effect and the induced-dipole potential of the atom by the laser field. We examine these effects carefully as well as other possible mechanisms.

5.1. Exchange effect

In all of our calculations, the interaction between the electron and Ar atom is described by a local model potential. The model potential has been parametrized to get the best agreement with the experimental field-free elastic scattering cross section. If the exchange effect participates in the scattering process, the cross section should have contained it and, in turn, this effect would be embedded in the model potential. To account for this effect more consistently and clearly, we have performed a frozen-core Hartree–Fock calculation. First, Hartree–Fock wavefunctions of the ground configuration of Ar are obtained self-consistently (Froese Fischer 1972). Exchange integrals are then included in constructing the $(N + 1)$ -electron Hamiltonian. The static exchange phase shifts, which are used in the KWA and the diabatic approximation, can be calculated from this Hamiltonian. The R -matrix calculation proceeds with the exchange Hamiltonian in place. The three methods show good agreement with each other.

The Hartree–Fock potential is not a good description of the electron–argon scattering and the cross section thus obtained does not compare well with the field-free experimental cross section. However, our purpose is to examine whether the exchange effect can dramatically increase the one-photon process where $\hat{\epsilon} \cdot \mathbf{Q}$ is small. According to the experiments, the one-photon process has a magnitude of about 1% to 10% of the elastic scattering for the perpendicular arrangement. Our calculations with the exchange effect show no such increase in the one-photon cross section. This rules out the possibility that the strong signals seen in the experiment are due to the exchange effect.

5.2. Laser-induced dipole potential

Outside the R -matrix boundary the Schrödinger equation has been completely transformed to the acceleration gauge and the electron–laser interaction disappears as a result. The atomic potential, however, is shifted by the time-dependent amplitude $(A_0/c\omega) \cos \omega t$ and provides residual coupling to the laser field. There are two different interactions arising because the electron cloud on the Ar atom can be polarized. One is the $\sim 1/r^4$ interaction of the outer electron with the dipole moment induced by the outer electron and the other one is the $\sim 1/r^2$ interaction of the outer electron with the dipole moment induced by the laser field. Although the latter diminishes more slowly than the electron-induced potential at large distances, its strength is much smaller. Explicitly the interaction of the electron with the laser-induced dipole is $\alpha_d E_0 \cos \theta \cos \omega t / r^2$ with $\alpha_d E_0 = 3.5 \times 10^{-4}$ au. It is therefore not surprising that we found no change in the cross section if this interaction is included inside the R -matrix boundary. Its slowly decaying character, however, requires some attention to the effect of this interaction on the T -matrix when the electron is outside of the boundary.

We calculated the effect on the cross section from the laser-induced dipole (i) by numerically solving the close-coupling equations with this potential and (ii) by using perturbation theory.

(i) High-angular-momentum states do not actively participate in the transition process inside the R -matrix boundary because of the centrifugal potential. We do not include high- l states in the R -matrix calculation because it is unnecessary and not practical. However, as we go further away from the atom, those high-angular-momentum states begin to mix in from the $1/r^2$ interaction. As a result, the number of coupled channels increases rapidly with the distance from the atom. For our calculation with the laser-induced dipole moment, we included the angular-momentum states up to $l = 25$ and used the diabatic approximation to obtain the T -matrix at 30 au. From this T -matrix we obtained channel wavefunctions and their derivatives at $r = 30$ au. The wavefunctions thus obtained served as the initial values for the coupled-channel equations to be solved outside of the boundary. The atomic potentials are transformed to the acceleration gauge which gives a correction to their forms in the length gauge; this additional factor is proportional to the ratio of the amplitude of oscillation to the distance of the electron from the origin in the acceleration gauge $(A_0/c\omega)/r$. The amplitude is 1.78 au and the correction term is only 6% compared to the leading terms at the R -matrix boundary. We keep only the leading terms followed by solving the close-coupled equations. The wavefunctions are propagated to 300 au and the full T -matrix (short range and long range) is constructed. If this laser-induced potential outside of the R -matrix boundary has a significant effect on the observed cross section, the procedure just described should give an estimate to the order of magnitude. We did not find a significant enhancement of the cross section.

(ii) According to the Kohn variational principle, the variational T -matrix element is given by

$$T_{j',j}^v = T_{j',j}^t - \pi \langle \psi_{j'}^t | V | \psi_j^t \rangle \quad (24)$$

where $T_{j',j}^t$ is obtained using the solution of a model Hamiltonian H_0 and $V = H - H_0$ with H the full Hamiltonian. The integration in the expression is to be performed over all space. For the present case, the R -matrix calculation has contained the dipole interaction inside r_0 ; the desired T -matrix can be more explicitly expressed as

$$T_{j',j} = T_{j',j}^R - \pi \int_{r_0}^{\infty} dr \int d\Omega \psi_{j'}^{t*} V_{\text{pol}} \psi_j^t \equiv T_{j',j}^R + T_{j',j}^P \quad (25)$$

where ψ_j^t is the wavefunction in the region $r \geq r_0$ for channel j and V_{pol} is the laser-induced dipole potential. A perturbative calculation approximates ψ_j^t by the solution of the Schrödinger equation assuming $V_{\text{pol}} = 0$ for $r \geq r_0$. This approximate wavefunction is given by (7) where the T -matrix is taken from the R -matrix calculation, $T_{j',j}^R$.

We found that $T_{j',j}^P$ slowly converges with respect to angular momentum. We note that in obtaining the differential cross section, the T -matrix has been summed over all the angular-momentum states in both the initial channel j and the final channel j'

$$T_{n_{j'}k_f, n_jk_i} = \sum_{l_{j'}m_{j'}l_jm_j} (i^{l_{j'}} Y_{l_{j'}m_{j'}}^*)^* T_{n_{j'}l_{j'}m_{j'}, n_jl_jm_j} (i^{l_j} Y_{l_jm_j}^*). \quad (26)$$

Since the short-ranged effect has vanished at large distances, the wavefunction deviates from the Bessel function only for low-angular-momentum states. We may expect $(T_{j',j}^R + T_{j',j}^P - T_{j',j}^B)$ contributes to the cross section only for low l where $T_{j',j}^B$ is the Born approximation. A fortunate property is that we can sum over all l and m analytically to get $T_{n_{j'}k_f, n_jk_i}^B$. The whole idea can be summarized as

$$T_{n_{j'}k_f, n_jk_i} = T_{n_{j'}k_f, n_jk_i}^B + \sum_{l_{j'}m_{j'}l_jm_j} (i^{l_{j'}} Y_{l_{j'}m_{j'}}^*)^* (T^R + T^P - T^B)_{n_{j'}l_{j'}m_{j'}, n_jl_jm_j} (i^{l_j} Y_{l_jm_j}^*). \quad (27)$$

We did not find a large enhancement of the cross section by this procedure.

It has been pointed out that at high incident electron energy a significant contribution to the free-free cross sections at small scattering angles comes from the dressing of the atom by the laser field (Byron *et al* 1984, 1987, Dörr *et al* 1994). These calculations have focused on the high-energy region and with larger electric field strength (about 600 times bigger than the present case). The dressing effect predicted for H and He atoms in the forward scattering is limited to small angles. We have used the perturbative procedure and parameters of the calculations on H to obtain the first Born cross section. There is a big enhancement in the forward direction for $\hat{\epsilon}$ parallel to the momentum transfer \mathbf{Q} and it is mainly from $T_{n_{j'}k_f, n_jk_i}^B$. The magnitude is proportional to Q_z/Q^2 and at the forward direction it reduces to $1/Q$. This is where the big effect comes from when Q is small. For the present case, the $1/Q$ contribution in the forward direction is reduced by a much weaker field strength in the experiment. Furthermore, in case 1 where \mathbf{k}_i is parallel to $\hat{\epsilon}$ and the scattering angle is between 9° and 25° , Q_z remains small but Q does not. The factor Q_z/Q^2 does not boost the cross section. It is also true for the perpendicular arrangement in which $\hat{\epsilon} \cdot \mathbf{Q} \approx 0$. $Q_z \approx 0$ but the magnitude Q is comparable to the electron momentum \mathbf{k}_i for large scattering angles. The dressing of the Ar atom by the laser field cannot explain the disagreement between calculations and experiments. Recently Geltman (1995) also examined this field-induced dipole effect and reached the same conclusion.

5.3. Other possibilities

Other possible explanations which could result in the discrepancies have also been considered. These include the possible misalignment of the equipment in scattering angles. This would make the perpendicularity in the momentum transfer and the polarization deviate from exactness. By intentionally shifting the scattering angle, we obtain a non-zero momentum transfer in the polarization direction which would favour the free–free transition. We find the shifted angle would need to be as large as 20° to account for the difference between experiment and theory and therefore is not a possible explanation.

Multiple scattering may be important if the density of the Ar beam in the experiment is relatively high. From the experiment (Weingartshofer *et al* 1983) the beam is about 0.5 mm in diameter and the pressure is 14 mTorr at the centre. The probability of double scattering under this condition is negligible. It is not likely the multiple scattering has an effect on the observed results.

We next consider the effect of experimental uncertainty in the laser intensity. The intensity of the laser field in our calculations ($3.8 \times 10^7 \text{ W cm}^{-2}$) is the first μs of the re-estimated value (Wallbank and Holmes 1994). The second and third μs are 1.3×10^7 and $0.42 \times 10^7 \text{ W cm}^{-2}$, respectively. These values are smaller than their previous estimated values $1.3 \times 10^8 \text{ W cm}^{-2}$ for the first μs and the second and third μs are $4.6 \times 10^7 \text{ W cm}^{-2}$ and $1.5 \times 10^7 \text{ W cm}^{-2}$ respectively. Suppose the average intensities were best described by the previous values: the intensity used in the calculation for the first μs is close to the second μs and larger than the third μs of the assumed set. If this were the case we should compare our results to the second μs of the experiment. However, the measurements of the experiment do not show much difference in signal for the first and second μs . We do not think the uncertainty in the average intensity can be the cause of the disagreement unless the actual intensity is several orders of magnitude larger than the estimation.

We did not include resonances in our calculations. The two lowest-resonant states of Ar^- , $^2\text{P}_{3/2}$ and $^2\text{P}_{1/2}$, lie at 11.1 and 11.27 eV, respectively with widths of $2.5 \pm 0.5 \text{ meV}$ (Brunt *et al* 1977). The energy of the incident electron is 8 eV and is more than 3 eV (1200 linewidths) away from the resonances. This suggests the resonances should not have any effect on the cross section where $\hat{\epsilon} \cdot \mathbf{Q} \approx 0$. This hypothesis can be tested using experimental data. If it is the resonances that cause the enhancement, the cross section at 10 eV, which is three times closer to the resonances, should be much larger than those at 8 eV. From the experiment, the magnitudes of the cross section at 10 eV and at 8 eV are about the same. This seems to rule out the resonances as the reason for the disagreement.

The laser field in our calculations is assumed to be single mode and spatially homogeneous. The pulsed CO_2 laser used in the experiments was used under multi-mode operation in which spatial and temporal averages are to be taken. The consequence of this is complicated and requires knowledge of the laser in the experiment. It is known that the trajectory of a charged particle in a laser field deviates from a straight line (Mittleman 1993). The scattering angles measured in the experiment may not correspond to the actual angles of the collision between the electron and the atom. If the field intensity is not homogeneous, it will change the electron's momentum. The correction to the momentum is a collective effect from the ponderomotive potential and its spatial variation in the scattering region. The ponderomotive potential is the difference between the kinetic energies of the electron inside and outside of the laser field. Its magnitude at the intensity in our calculations is $U_p = E_0^2/4\omega^2 = 1.47 \times 10^{-5} \text{ au}$ if the field is homogeneous. This is negligibly small compared to the kinetic energy 8 eV ($\sim 0.294 \text{ au}$) outside of the laser field. Unless the laser intensity has strong spatial nonhomogeneity in the scattering region, the electron will not change paths because of the inhomogeneity of the laser field.

5.4. Validity of the KWA

The KWA is believed to be valid when the photon energy of the laser field is smaller than both the energy of the incident electron and the excitation energy of the target atom. These conditions are well satisfied with 8 eV incident electrons in the experiments. The R -matrix method is not only an alternative method to the KWA, it also provides a tool to examine the validity of the KWA. They are complementary in that while the KWA is applicable to the low-frequency limit, the R -matrix approach is valid provided $A_0/c\omega$ is small compared to the R -matrix size. This is usually satisfied in the high-frequency region where the KWA tends to fail. It is desirable to use the R -matrix method to test the limit of the validity of the KWA.

Since the validity conditions for KWA are in good standing in the above calculations, we choose a high frequency $\omega = 0.25$ au to explore its limit and still keep the incident energy of the electron at 8 eV. The photon energy is no longer small compared to the incident energy and $n = -2$ is now a closed channel. The high frequency also allows us to increase the intensity to 3.8×10^{12} W cm⁻² with the amplitude $A_0/c\omega = 0.17$ au which is tiny compared to the size of the R -matrix boundary at $r = 30$ au. Even under this condition we found that the KWA prediction of the cross section is fairly close to the R -matrix except for the ‘perpendicular’ arrangement. The largest difference occurs in the $n = -1$ channel which is 1.2 eV above threshold. In this channel the R -matrix results show much larger cross section than the KWA. If the arrangement is ‘perpendicular’, their differences are more apparent. Because the photon energy is comparable to the incident energy, $\hat{\epsilon} \cdot \mathbf{Q} \approx 0$ even when the polarization direction bisects the angle between the directions of the incident electron and the scattered electron (‘perpendicular’ arrangement). Overall, the validity of the KWA seems to go beyond its usual criteria.

5.5. Peculiar symmetry in the diabatic approximation

We have mentioned the one-photon differential cross section from the diabatic approximation is exactly zero if $\hat{\epsilon} \cdot \mathbf{Q} = 0$. Actually all n -photon differential cross sections vanish for this approximation if n is odd. This is an exclusive feature of the diabatic approximation and comes from indistinctness of channel index n in (13). The index n comes in to play in the time average of (17). Because $T_{L,L'}^m(t)$ is symmetric about $t = 0$, there is no difference between n -photon absorption and emission processes as mentioned earlier. In calculating the differential cross section, we need to perform the summation in (26). The independent indices L and L' form pairs in the summation, e.g. for one term with $L = 1, L' = 2$ there is another term with $L = 2, L' = 1$. While the product of spherical harmonics $Y_{L,m} \times Y_{L',m}^*$ and $T_{nL,n'L'}^m$ remain unchanged with the exchange of L and L' , the phase factor $i^{L'-L}$ changes sign if $L' - L = \pm 1, \pm 3, \dots$. The summation over L and L' for these pairs have a perfect cancellation for a given m . Terms with $L' - L = 0, \pm 2, \pm 4, \dots$ will add up because the factors $i^{L'-L}$ and $i^{L-L'}$ have the same sign. However, we found $T_{nL,n'L'}^m = 0$ for odd n but $T_{nL,n'L'}^m \neq 0$ for even n . Hence, for odd n , all terms add up to zero. This does not happen for the R -matrix calculation because the absorption and emission have different channel energies. For even n this symmetry does not hold. However, as mentioned before, by including more angular-momentum states, the differential cross section eventually vanishes. Thus, in the diabatic approximation, no n -photon (except $n = 0$) free-free transitions occur if $\hat{\epsilon} \cdot \mathbf{Q} = 0$. This conclusion should not be taken too seriously because the additional simplifications of the method. However, at low frequencies where the diabatic assumption is a good approximation, this conclusion should be approximately right and we can expect small laser-assisted signals under the experimental conditions discussed above.

6. Conclusions

We have presented a non-perturbative R -matrix Floquet calculation and a diabatic approximation to the differential and total cross section of electron–argon scattering in a low-frequency CO₂ laser. The calculations attempted to explain recent experiments by Wallbank and Holmes. We have found that these calculations agree with the Kroll–Watson approximation but do not agree with the observed strong signals in the forward direction and in the case where the electron momentum transfer is perpendicular to the direction of the laser polarization. This conclusion agrees with some previous results (Geltman 1995, Varró and Ehlötzky 1995). Several possible explanations for the discrepancy have been examined but excluded. This seems to suggest that some of the assumptions in the calculations do not correspond to the real experimental conditions. We also present the total cross sections as a function of incident and scattered angle. Our calculations, though unable to explain the experiments, should provide valuable information for further investigation of this problem.

Acknowledgments

The authors would like to acknowledge Dr L A Collins for informative conversations. This work is supported in part by an NSF Young Investigator grant (NSF-PHY-9457903) with Auburn University.

References

- Bader H 1986 *J. Phys. B: At. Mol. Phys.* **19** 2177
Brunt J N H, King G C and Read F H 1977 *J. Phys. B: At. Mol. Phys.* **10** 1289
Byron F W Jr, Francken P and Joachain C J 1987 *J. Phys. B: At. Mol. Phys.* **20** 5487
Byron F W Jr and Joachain C J 1984 *J. Phys. B: At. Mol. Phys.* **17** L295
Daniele R, Ferrante G, Morales F and Trombetta F 1986 *J. Phys. B: At. Mol. Phys.* **19** L133
Daniele R, Trombetta F and Ferrante G 1987 *Phys. Rev. A* **36** 1156
Danos M and Maximon L C 1965 *J. Math. Phys.* **6** 766
Dill D and Dehmer J L 1974 *J. Chem. Phys.* **61** 692
Dörr M, Burke P G, Joachain C J, Noble C J, Purvis J and Terao-Dunseath M 1993 *J. Phys. B: At. Mol. Opt. Phys.* **26** L275
Dörr M, Joachain C J, Potvliege R M and Vučić S 1994 *Phys. Rev. A* **40** 5592
Dörr M, Terao-Dunseath M, Burke P G, Joachain C J, Noble C J and Purvis J 1995 *J. Phys. B: At. Mol. Opt. Phys.* **28** 3545
Dörr M, Terao-Dunseath M, Purvis J, Noble C J, Burke P G and Joachain C J 1992 *J. Phys. B: At. Mol. Opt. Phys.* **25** 2809
Fainstein P D and Maquet A 1994 *J. Phys. B: At. Mol. Opt. Phys.* **27** 5563
Fon W C, Berrington K A, Burke P G and Hibbert A 1983 *J. Phys. B: At. Mol. Phys.* **16** 307
Froese Fischer C 1972 *Comput. Phys. Commun.* **4** 107
Furst J E, Mahgerefteh M, Zhou J and Mueller D 1989 *Phys. Rev. A* **40** 5592
Geltman S 1995 *Phys. Rev. A* **51** R34
Greene C H 1985 *Phys. Rev. A* **32** 1880
Johnson W, Kohb D and Huang K N 1983 *At. Data Nucl. Data Tables* **28** 333
Kroll N M and Watson K M 1973 *Phys. Rev. A* **8** 804
Mason N J 1993 *Rep. Prog. Phys.* **56** 1275
McEachran R P and Stauffer A D 1983 *J. Phys. B: At. Mol. Phys.* **16** 4023
Mittleman M H 1993 *Introduction to the Theory of Laser–Atom Interactions* 2nd edn (New York: Plenum) pp 114–9
Rabadán I, Méndez L and Dickinson A S 1994 *J. Phys. B: At. Mol. Opt. Phys.* **27** L535
Robicheaux F 1991 *Phys. Rev. A* **43** 5946
Robicheaux F, Chen C T, Gavras P and Pindzola M S 1995 *J. Phys. B: At. Mol. Opt. Phys.* **28** 3047

Schneider B I 1975 *Chem. Phys. Lett.* **31** 237

Varró S and Ehlötzky F 1995 *Phys. Lett.* **203A** 203

Wallbank B and Holmes J K 1993 *Phys. Rev. A* **48** R2515

— 1994a *J. Phys. B: At. Mol. Opt. Phys.* **27** 1221

— 1994b *J. Phys. B: At. Mol. Opt. Phys.* **27** 5405

Weingartshofer A, Holmes J K, Sabbagh J and Chin S L 1983 *J. Phys. B: At. Mol. Phys.* **16** 1805

Williams J F 1979 *J. Phys. B: At. Mol. Phys.* **12** 265